Lowering the Barriers to Random Walks on the Cell Surface

Qing Tang and Michael Edidin
Department of Biology, The Johns Hopkins University, Baltimore, Maryland 21218-2685 USA

ABSTRACT We used fluorescence recovery after photobleaching (FRAP) and single particle tracking (SPT) techniques to compare diffusion of class I major histocompatibility complex molecules (MHC) on normal and α-spectrin-deficient murine erythroleukemia (MEL) cells. Because the cytoskeleton mesh acts as a barrier to lateral mobility of membrane proteins, we expected that diffusion of membrane proteins in α-spectrin-deficient MEL cells would differ greatly from that in normal MEL cells. In the event, diffusion coefficients derived from either FRAP or SPT analysis were similar for α-spectrin-deficient and normal MEL cells, differing by a factor of $\sim$2, on three different timescales: tens of seconds, 1–10 s, and 100 ms. SPT analysis showed that the diffusion of most class I MHC molecules was confined on both cell types. On the normal MEL cells, the mean diagonal length of the confined area was 330 nm with a mean residency time of 40s. On the α-spectrin-deficient MEL cells, the mean diagonal length was 650 nm with a mean residency time of 45s. Thus there are fewer barriers to lateral diffusion on cytoskeleton mutant MEL cells than on normal MEL cells, but this difference does not strongly affect lateral diffusion on the scales measured here.

INTRODUCTION

Many studies have shown that the lateral mobility of membrane proteins is hindered (Edidin, 2001; Saxton and Jacobson, 1997; Kusumi et al., 1993), creating a patchy membrane with heterogeneous distribution of its components. The models proposed to interpret the data on patchiness emphasize the role of the cytoskeleton underlying the membrane in restricting lateral diffusion (Sheetz, 1983; Tsuji et al., 1988; Tsuji and Ohnishi, 1986). The cytoskeleton meshwork compartmentalizes the membrane into many small domains. Diffusion in these domains is effectively limited by lipid viscosity and by interactions with other membrane proteins (Tomishige et al., 1998), but diffusion on a scale larger than the size of a domain (hundreds of nm) depends both on these factors and on the frequency with which a diffusing molecule can cross the cytoskeleton fences that create the domains. We expect then that mutations that create defects in the organization of the cytoskeleton will change the lateral mobility observed for membrane proteins on the mutant cells.

The cytoskeleton of erythrocytes is the best-characterized cytoskeleton and most accessible to biochemical and genetic manipulation. It has often been used to study the role of cytoskeleton in the membrane dynamics (Bennett and Gilligan, 1993; Cherry, 1979; Koppel and Sheetz, 1981; Koppel et al., 1981; Schindler et al., 1980; Sheetz et al., 1980). The cytoskeleton has a lattice-like organization of five- or six-sided polygons. A flexible rod-shaped protein, spectrin, forms the legs of the polygons. Short actin filaments form the vertices of the network (Bennett and Gilligan, 1993). Spectrin and actin require accessory proteins to form membrane-associated network. A major membrane attachment is provided by high affinity association of the β-spectrin with ankyrin (Bennett and Gilligan, 1993). Both fluorescence recovery after photobleaching (FRAP) and single particle tracking (SPT) have given clear results on the effects of membrane skeleton fences on lateral diffusion in erythrocytes. High speed SPT of erythrocytes shows that small-scale lateral diffusion of membrane proteins is limited by membrane lipid viscosity (Tomishige at al., 1998). FRAP measurements of erythrocytes also imply this result, because observed diffusion of membrane proteins increases 10- to 50-fold in erythrocytes with deficiency in cytoskeleton (Corbett et al., 1994; Golan and Veatch, 1980; Sheetz et al., 1980; Tsuji and Ohnishi, 1986).

Erythrocytes are nonmotile end cells, and this may limit the applicability of studies of diffusion in erythrocyte membranes. Also, the cells are not easy to use for many techniques for characterizing lateral mobility of membrane proteins, ranging from antibody-induced capping to single particle tracking. To address this problem, we created murine erythroleukemia (MEL) cell lines from erythroid precursors of mice deficient in α-spectrin (Dahl et al., 1994). These nucleated, motile cells could be used to study membrane dynamics. We found that capping of class I major histocompatibility complex (MHC) molecules was 5–10 times faster on the mutant cells than on cells expressing α-spectrin (Dahl at al., 1994). This implied that barriers to lateral mobility on a micrometer scale were lower in α-spectrin-deficient cells than in normal cells. However, these experiments did not speak to barriers on smaller scales, hundreds of nm. Also, because capping is an ATP-driven process, the capping result only speaks to barriers crossed by high energy lateral movements and do not necessarily show that status of barriers to Brownian motion in the plane of the membrane.

We explored lateral diffusion of class I MHC molecules on α-spectrin-MEL cells using SPT (Qian et al., 1991; Saxton and Jacobson, 1997; Smith et al., 1999). In contrast to the FRAP technique commonly used to measure diffusion coefficients in

Submitted May 23, 2002, and accepted for publication September 14, 2002.

Address reprint requests to Michael Edidin, E-mail: edidin@jhu.edu.

0006-3495/03/01/400/08 $2.00

a large ensemble of molecules and a distance of ~1 μm, SPT monitors the lateral diffusion of single or few membrane proteins labeled by an antibody-coated bead, typically 20–50 nm diameter. SPT probes lateral diffusion with a temporal resolution of 33 ms (for real time video microscopy) or faster (Tomishige at al., 1998) at a spatial scale of tens of nm. If lateral diffusion is constrained by cytoskeleton fences, SPT also reports on the area of fenced domains.

To our surprise we found that class I MHC molecules were as frequently confined in compartments on the membrane of α-spectrin-deficient MEL cells as on normal MEL cells. Lateral diffusion coefficients on two scales were also close, differing only by a factor of ~2. The biggest difference between α-spectrin-deficient MEL cells and MEL cells with normal membrane skeleton was in the size of compartments confining diffusion. The area of these compartments in α-spectrin-deficient MEL cells was about four times that of compartments in normal cells. Thus, major defects in the spectrin/actin cytoskeleton, defects that change global properties of the mutant cells, have relatively small impact on plasma membrane compartmentation, at least as sensed by class I MHC molecules. This suggests that other factors such as anchored transmembrane proteins constrain lateral diffusion in the absence of a fully organized membrane skeleton (Fujiwara et al., 2002).

MATERIALS AND METHODS

Cell cultures and antibody

Normal and α-spectrin-deficient MEL cells (Dahl at al., 1994) were cultured at 37°C in RPMI 1640 medium with L-glutamine (Mediatech, Herndon, VA), with 10% heat inactivated fetal bovine serum (FBS) (Life Technologies, Grand Island, NY), and 100 U/ml antibiotic/antimycotic (Life Technologies). HEPA-OVA cells expressing 2.2.1 mutant class I MHC molecules (Edidin et al., 1994) were cultured at 37°C in Dulbecco's modified Eagle's medium (Mediatech) with 10% heat inactivated FBS, 100 U/ml antibiotic/antimycotic (Life Technologies), and 400 μg/ml G418 (Geneticin, Sigma, St Louis, MO). H-2L^d-specific monoclonal antibody (mAb), 28.14.8 IgG, was purified over protein A column (Sigma) from the medium containing ATCC HB27 hybridoma cell secretion (Ozato et al., 1980). Fab fragments were prepared by papain digestion as described previously (Edidin and Stroynowski, 1991).

Fluorescence recovery after photobleaching

Cy3 (Amersham Biosciences) was conjugated to 28.14.8 Fab at 1:1 ratio according to Amersham Biosciences' protocol. MEL cells were washed in phosphate-buffered saline and incubated with Cy3-28.14.8 Fab conjugates at 4°C for 30 min. Then cells were washed three times in phosphate-buffered saline and resuspended. Cells were put on the poly-L-lysine coated coverslip and allowed to attach to the coverslip for 5 min at room temperature before the coverslip was mounted on a microscope slide. An air stream incubator (ASI-400, NevTek, Burnsville, VA) was used to maintain the sample at 37°C. A homemade FRAP setup was used to determine the lateral diffusion coefficient of class I MHC molecules on the cell surface membrane at 37°C (Axelrod et al., 1976; Edidin and Wei, 1982; Edidin et al., 1976; Jacobson et al., 1976; Wolf et al., 1980). In brief, an attenuated laser beam with 0.8 μm radius was used to monitor the fluorescence intensity of the selected membrane area all the time. A brief bleach laser beam (8–50 ms) was used to bleach 20–80% fluorescence of that area. Fluorescence recovery after the bleach was recorded for 60–120 s. The lateral diffusion coefficient of class I MHC molecules was determined from the fluorescence recovery curve as described (Wolf, 1989).

FRAP experiments with different laser spot sizes by using difference objectives were also done on the same sample to see the effect of spot size on the measured mobile fraction. The diffusion coefficients of class I MHC on cells labeled with Cy3-28.14.8 Fab-conjugated latex bead (50 nm, Polysciences, Warrington, PA) or Cy3-Fab were also measured by FRAP.

Preparation of carboxylate latex bead-Fab conjugate

Fluoresbrite carboxylate latex beads (50 nm, Polysciences) were used for SPT. Beads were coated with 28.14.8 Fab at 1:1 ratio. In brief, an aliquot of the beads (0.5 ml, 3.6×10^{14} beads/ml) was sonicated and incubated at room temperature with 0.1 ml 28.14.8 Fab stock solution (3 μM), which also had the same amount of molecules (1.8×10^{14}) for 2 h. Then 0.2 ml BSA (20 mg/ml) was added to the mixture to coat the surface of the beads. The bead-Fab conjugates were separated from Fab by passing the mixture through Sephadex G-200 (Amersham Biosciences).

Flow cytometry

Analytical flow cytometry was used to test whether the bead-Fab conjugates specifically bind class I MHC molecules on the cell surface. HEPA-OVA cells transfected with 2.2.1 mutant class I MHC molecules were trypsinized and centrifuged at $300 \times g$ for 5 min at room temperature. Then cells were washed in Hepes-buffered Hanks' containing 2% FBS three times. Bead-Fab conjugates, bead only, or excess mAb first, followed by bead-Fab conjugates were incubated with cells for 30 min at room temperature, respectively. Cells were then washed three times with Hepes-buffered Hanks' containing 2% FBS and resuspended. The fluorescence was examined by a Coulter EPICS 752 cytometer (Beckman Coulter, Miami, FL) equipped with Cytomation Cyclops software (Cytomation, Fort Collins, CO), counting 10,000 cells.

Fluorescence video microscopy

Poly-L-Lysine coated coverslips

Coverslips (22 × 22 cm, Fisher Scientific, Pittsburgh, PA) were cleaned with ethanol and washed thoroughly with double-distilled H_2O. The coverslips were then immersed in poly-L-lysine (0.01% w/v, 1:10 dilution from stock solution from Sigma) for 10 min at room temperature. Then coverslips were dried overnight at room temperature.

Bead-Fab conjugates on cells

Normal MEL and mutant MEL cells were centrifuged at $300 \times g$ for 5 min. Cells were resuspended in 0.5 ml Hepes-buffered Hanks' containing 2% FBS and incubated with 0.2 ml bead-Fab at 4°C for 30 min. Then cells were washed three times with Hepes-buffered Hanks' containing 2% FBS. Cells were put on the poly-L-lysine-coated coverslip and allowed to attach to the coverslip for 5 min at room temperature before the coverslip was mounted on a microscopy slide. An ASI air stream incubator was used to maintain the sample at 37°C.

Video microscopy

Real-time videos were recorded from an intensified CCD camera (I-PentaMAX, Roper Scientific, Trenton, NJ) installed on a Zeiss Axiovert 135-TV conventional inverted microscope (Carl Zeiss, Thornwood, NY) with a 100 × 1.4 NA oil DIC objective (Plan-Apochromat, Zeiss) and a 75

W xenon arc lamp epiillumination. The video frame resolution is 704 × 480 pixels corresponding to 47.2 nm/pixel for x axis and 52.8 nm/pixel for y axis with the 100× objective and a 2.5 amplifier lens. Each video sequence was tracked for 2 min and ~30 video sequences for each type of cell were recorded.

Data analysis

SPT through video sequences

Video sequences were digitized to AVI format movies by using a video capture card (Maruel 6400-TV, Matrox Graphics, Dorval, Canada). Then each frame in the AVI movie was saved as a TIFF image using QuickTime software (Apple, Cupertino, CA). The TIFF image sequences were imported into ISee software (version 5.0, ISee Imaging System, Raleigh, NC) and particles were identified and tracked by the NanoTrack module in this software. In brief, the software tracks the centroid of a given particle through the image sequence and saves the position of each particle (x and y coordinates) in a text file.

Mean square displacement

From each particle's position in successive images, the mean square displacement (MSD) was calculated according to the equation:

$$\mathrm{MSD}(\Delta t_n) = \mathrm{MSD}(n\delta t) = \sum_{j=1}^{N-1-n} \{[x(j\delta t + n\delta t) - x(n\delta t)]^2 + [y(j\delta t + n\delta t) - y(j\delta t)]^2\} \quad (77)$$

where δt is video rate, 33 ms; $(x(j\delta t + n\delta t), y(j\delta t + n\delta t))$ is the particle position after starting at position $(x(j\delta t), y(j\delta t))$ for a time interval $\Delta t_n = n\delta t$; N is the total number of frames in the video sequence; and n and j are positive integers, with n determining the time increment (Kusumi et al., 1993; Lee et al., 1991; Qian at al., 1991). We used internal averaging and one-quarter of the total number of data points because there are not enough data points at large time lags to give a reliable value of the MSD (Saxton, 1997).

Determining microscopic diffusion coefficient

A microscopic diffusion coefficient (D_{micro}) was determined by a linear fit to the MSD curve at $2\delta t$, $3\delta t$, and $4\delta t$ (Kusumi at al., 1993). This method is independent of diffusion modes.

Determining macroscopic diffusion coefficient

The macroscopic diffusion coefficient (D_{macro}) was calculated by ensemble-averaging all MSD curves and then fitting the average to a linear function. Whereas D_{micro} describes diffusion of a particle in the ~100 ms time range, D_{macro} describes diffusion in a few seconds to tens of seconds time range. Of course, D_{micro} and D_{macro} also are in different spatial scales.

Determining diffusion modes

The relative deviation, $RD(N,n)$ is defined as:

$$\mathrm{RD}(N,n) = \frac{\mathrm{MSD}(N,n)}{4D_{micro}n\delta t} \quad (77)$$

where $MSD(N,n)$ represents MSD determined at a time interval $n\delta t$ from a sequence of N video frames. $4D_{micro}n\delta t$ is the expected average value of MSD for particles undergoing simple two-dimensional diffusion with a diffusion coefficient of D_{micro} (Kusumi at al., 1993). In the case of simple diffusion, the average $RD(N,n)$ should be 1. For computer-simulated simple diffusion, given N and n, 95% of the $RD(N,n)$ distribution lies between $RD(N,n)_{max}$ and $RD(N,n)_{min}$ with only 2.5% of the particles smaller than $RD(N,n)_{min}$ and 2.5% bigger than $RD(N,n)_{max}$, respectively (Kusumi at al., 1993). If the experimental particle's $RD(N,n)$ value is greater than $RD_{max}(N,n)$, between $RD_{max}(N,n)$ and $RD_{min}(N,n)$, or smaller than $RD_{min}(N,n)$, this particle is classified as having directed, simple Brownian or restricted diffusion mode, respectively (Kusumi, 1993), with 95% certainty. In our analysis, we fixed n at 90. Because we have different total numbers of frames for each particle track, we used various N. We removed all particles with N smaller than 300 frames, due to the noise of $RD(N,90)$ in these short sequences. We then calculated the $RD(N,90)$ for all the remaining particles, and sorted them into three diffusion modes, according to the criteria of Kusumi, for $RD_{max}(N,90)$ and $RD_{min}(N,90)$ (Fig. 7 A in Kusumi et al., 1993).

Determining domain size

In restricted diffusion mode, the particle diffuses within a limited area during the observation period ($0 \le x \le Lx$, $0 \le y \le Ly$). The domain size was calculated as the diagonal length of the area, $(L_x^2 + L_y^2)^{1/2}$.

RESULTS

Lateral diffusion coefficients determined by FRAP

Both normal and mutant MEL cells were labeled with Cy3-mAb and the lateral diffusion coefficients were measured by FRAP. The FRAP method could not distinguish between the lateral diffusion of class I MHC molecules on these two types of cells on the length scale of micrometers and timescale of tens of seconds. The mean diffusion coefficients of class I MHC molecules on normal MEL and α-spectrin-deficient MEL cells were 0.06 ± 0.02 $\mu m^2/s$ (Fig. 1 C) and 0.07 ± 0.02 $\mu m^2/s$ (Fig. 1 A), respectively. The mobile fractions

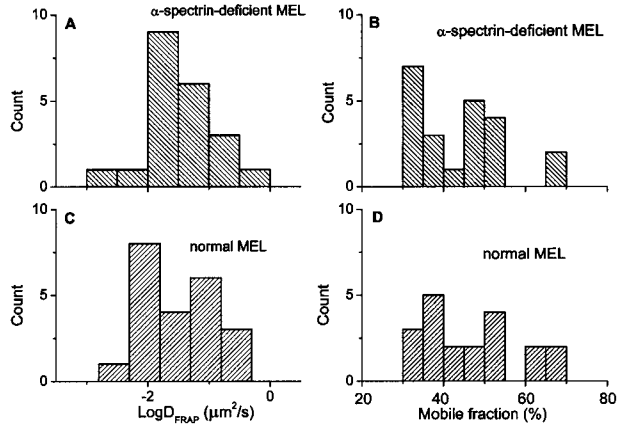

FIGURE 1 Diffusion coefficients (D_{FRAP}) and mobile fractions of class I MHC molecules measured by FRAP. (A) D_{FRAP} of α-spectrin-deficient MEL cells; (B) mobile fraction of α-spectrin-deficient MEL cells; (C) D_{FRAP} of normal MEL cells; (D) mobile fraction of normal MEL cells. In A and C, x axis is logarithmic scale.

were 44 ± 17% (Fig. 1 *B*) and 45 ± 19% (Fig. 1 *B*) on normal MEL and α-spectrin-deficient MEL cells, respectively.

FRAP measurements with different radii can detect membrane domains that are stable on the FRAP timescale, tens of seconds. If domains are present, the mobile fraction of labeled molecules decreases with increasing spot radius (Yechiel and Edidin, 1987). We found this to be the case for both normal and α-spectrin-deficient MEL cells (Table 1). It appears that the change in mobile fraction with spot size was smaller for mutant cells than for normal cells, suggesting that average domain size was larger in the mutant cells. This hint from FRAP data was borne out by SPT results.

As a calibration for measuring D by SPT, FRAP experiments were done on cells labeled with Cy3-28.14.8 Fab-conjugated latex beads or Cy3-28.14.8 Fab. The measured D of molecules labeled with Fab-coated beads was twofold to threefold smaller than the D of those labeled with Fab: 0.03 ± 0.01 $\mu m^2/s$ on α-spectrin-deficient MEL cells and 0.02 ± 0.01 $\mu m^2/s$ on normal MEL cells.

Bead-Fab specificity

The specificity of the bead-Fab for class I MHC molecules was tested by flow cytometry. Flow cytometric analysis showed that there was high fluorescence intensity from the cells after the cells were incubated with bead-Fab. However, when incubated either with beads only, or with excess mAb first, followed by bead-Fab, cells fluorescence was almost as low as that of the control, unlabeled cells (data not shown).

Macro- and microscopic diffusion coefficients determined by SPT

Both normal and mutant MEL cells were labeled with Fab-coated beads. Single particles were tracked and MSD curves were generated for the particles, as described in Materials and Methods. Some sample tracks are shown in Fig. 2. The D_{macro} was determined from ensemble-averaged MSD curves for all the particles. On normal MEL cells, D_{macro} of class I MHC molecules was 0.004 $\mu m^2/s$ (Fig. 3 *C*), whereas on α-spectrin-deficient MEL cells, D_{macro} was 0.007 $\mu m^2/s$ (Fig. 3 *A*). D_{macro} measures the average diffusion coefficient of many class I MHC molecules on a micrometer spatial scale and a timescale of seconds to tens of seconds. D_{micro} were determined by fitting the $2\delta t$ to $4\delta t$ of the MSD curve with a straight line (Kusumi at al., 1993). On normal MEL cells, the D_{micro} of class I MHC molecules was 0.007 $\mu m^2/s$ ± 0.002 (Fig. 3 *D*), whereas on α-spectrin-deficient MEL cells, the D_{micro} was 0.02 ± 0.005 $\mu m^2/s$ (Fig. 3 *B*). So D_{FRAP} of Fab-labeled molecules is twofold to threefold bigger than D_{FRAP} of bead-labeled molecules, which is close to the D_{micro} of bead-labeled molecules mea-

TABLE 1 FRAP data for normal and mutant MEL cells, using various objectives

		Mobile fraction (%)				Diffusion coefficient ($\mu m^2/s$)			
		Normal MEL		Mutant MEL		Normal MEL		Mutant MEL	
Objectives	R* (μm)	Mean	± SD	Mean	± SD	Mean†	±c‡	Mean†	±c‡
20×	0.8	19	7	27	6	0.13	0.02	0.13	0.02
40×	0.6	34	15	40	17	0.08	0.02	0.06	0.02
60×	0.4	44	17	45	19	0.06	0.02	0.07	0.02
100×	0.35	42	13	43	11	0.03	0.01	0.03	0.01

*R is the spot radius at $1/e^2$ laser maximum intensity.
†This is geometric mean. All other means without this footnote are arithmetic mean.
‡This is the 95% confidence interval from geometric mean.

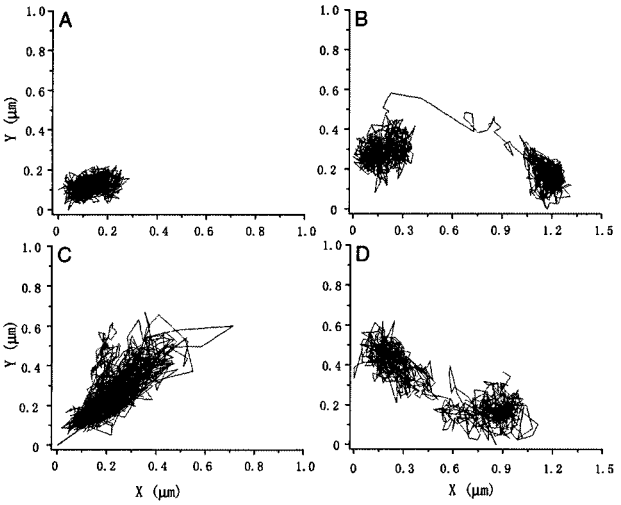

FIGURE 2 Sample particle tracks of SPT. (*A* and *B*) normal MEL cells; (*C* and *D*) α-spectrin-deficient MEL cells. Duration for each track: (*A*) 14 s; (*B*) 51 s; (*C*) 55 s; (*D*) 34 s.

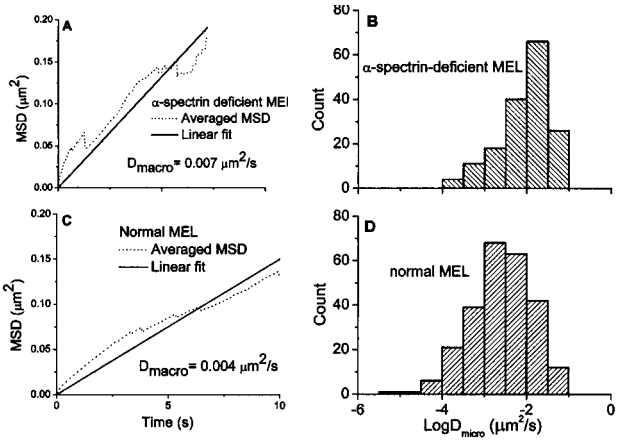

FIGURE 3 Macroscopic diffusion coefficients (D_{macro}) and microscopic diffusion coefficients (D_{micro}) measured by SPT. (*A*) D_{macro} of α-spectrin-deficient MEL cells; (*B*) D_{micro} of α-spectrin-deficient MEL cells; (*C*) D_{macro} of normal MEL cells; (*D*) D_{micro} of normal MEL cells. In *A* and *C*, the dotted line is the ensemble average of all MSD curves, and the solid line is the linear fit passing the origin (0,0). In *B* and *D*, *x* axis is logarithmic scale.

TABLE 2 Comparison of diffusion coefficients of class I MHC molecules on normal MEL and α-spectrin-deficient MEL measured by FRAP and SPT

	FRAP (μm^2/s) Fab			FRAP (μm^2/s) Bead			SPT (μm^2/s)			
	Mean*	±c†	n‡	Mean*	±c†	n‡	D_{macro}§	D_{micro}*	±c†	n‡
Normal	0.06	0.02	25	0.02	0.01	20	0.004	0.007	0.002	262
Mutant	0.07	0.02	25	0.03	0.01	20	0.007	0.02	0.005	171

*This is geometric mean.
†This is the 95% confidence interval from geometric mean.
‡Experiment or particle number.
§Because D_{macro} was calculated from ensemble averaging, there was no SD.

sured by SPT. D_{micro} by SPT is another twofold to threefold bigger than D_{macro} by SPT (Table 2).

The low diffusion coefficient was characteristic of MEL cells. When SPT was used to measure D of class I MHC molecules on HEPA-OVA cells, D_{micro} of class I MHC molecules was ~0.14 μm^2/s measured either with antibody-coated gold beads (Zuniga et al., unpublished) or with antibody-coated latex beads.

Diffusion modes

Relative deviation (RD) defines the deviation of an experimental particle's MSD curve from the theoretical MSD curve for simple diffusion. In the computer simulation of simple diffusion (Kusumi at al., 1993), particles corresponding to the middle 95% of the RD distribution are classified as in the simple diffusion mode. Particles with RD in the lowest 2.5% of the distribution ($<RD_{min}$) are classified as undergoing restricted diffusion; particles with RD in the highest 2.5% of the distribution ($>RD_{max}$) are classified as undergoing directed diffusion. In our experiments, the RD for each particle was calculated and plotted against N, the total frames tracked for a given particle (Fig. 4). Two limiting curves, RD_{max} and RD_{min} from Kusumi's simulation (Kusumi at al., 1993) were added to the plot. Particles with (RD,N) falling above the RD_{max} limit were classified as directed diffusion. Similarly, particles with (RD,N) falling below the RD_{min} limit were classified as restricted diffusion. Particles with (RD,N) falling within the limits represented simple diffusion. The fractions of restricted diffusion, simple diffusion, and directed diffusion for labeled class I MHC molecules on normal MEL cells were 85%, 13%, and 2%. The fractions of restricted diffusion, simple diffusion, and directed diffusion for labeled class I MHC molecules on α-spectrin-deficient MEL cells were 82%, 16%, and 1%. Thus restricted or confined diffusion was the principal form of Brownian motion on both types of cells. However, the average area of confinement of a particle was four times larger on α-spectrin-deficient MEL cells (Fig. 5 *A*) than on normal MEL cells (Fig. 5 *B*). The mean average confinement area of the particles on normal MEL cells was 0.057 ± 0.006 μm^2, or a mean diagonal length of 330 ± 80 nm (Fig. 5 *B*). The mean average confinement area of the particles on α-spectrin-deficient MEL cells was 0.21 ± 0.02 μm^2, or a mean diagonal length of 650 ± 150 nm (Fig. 5 *A*). The mean residency time in a confinement area was 40 ± 27 s

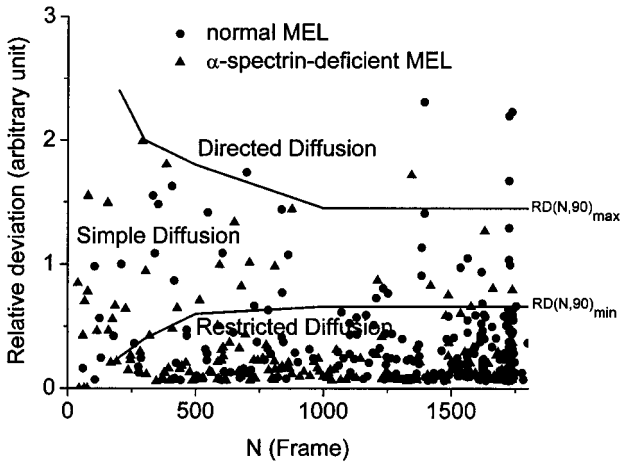

FIGURE 4 Relative deviations for all the particles. N is the number of total frames tracked for each particle. $RD(N,90)$ was calculated for each particle (see Materials and Methods). ($RD(N,90)$, N) plots were separated into three diffusion modes by two curves (Kusumi et al., 1993).

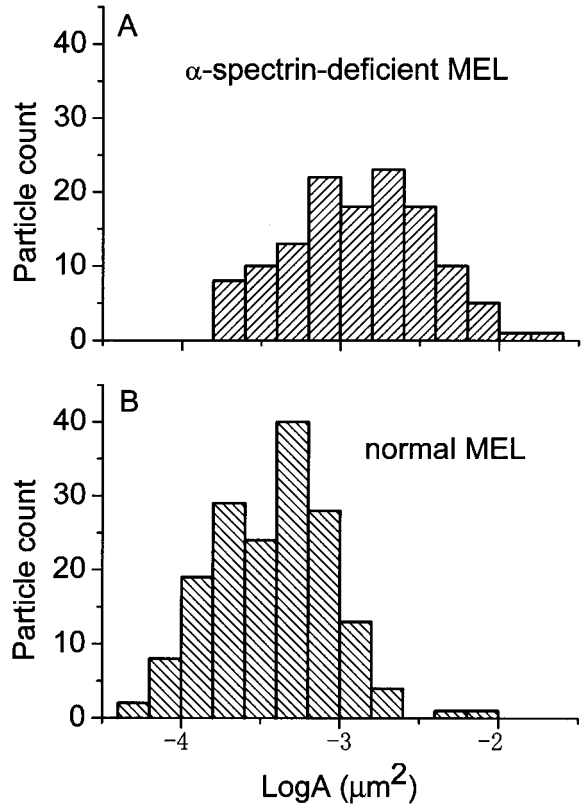

FIGURE 5 Area swept in the cell membrane by restricted diffusion particles. (*A*) α-spectrin-deficient MEL cells; (*B*) normal MEL cells. X axis is logarithmic scale.

on normal MEL cells and 45 ± 32 s on α-spectrin-deficient MEL cells.

Anomalous diffusion analysis

MHC class I has been shown to undergo anomalous diffusion on HeLa cells (Georgiou et al., 2002; Smith et al., 1999). To check if our data can be fit by anomalous diffusion, plots of $\log[<r^2>/t]$ against $n\delta t$ were generated as recommended by Saxton (1994) (Fig. 6). In Fig. 6, *E* and *F*, the linear fit of the beginning part of the curve gives us a slope $(\alpha-1)$ with a mean anomalous exponent of $\alpha = 0.50 \pm 0.21$ for normal MEL cells and $\alpha = 0.28 \pm 0.13$ for α-spectrin-deficient MEL cells. However, as analyzed by Saxton, the tail part of the curve can be fit to a horizontal line that indicates normal diffusion. The crossover point of these two linear fits indicates the crossover time between anomalous diffusion and normal diffusion. In our case, it seems that within 5 s on normal MEL cells, or within 8 s on α-spectrin-deficient MEL cells, diffusion of particles is anomalous diffusion. On a larger timescale, the diffusion is normal diffusion. This is also verified by the fact that more than 80% of the restricted diffusion MSD curves showed distinct plateaus over long time range, which implies restricted diffusion, not anomalous diffusion (Saxton and Jacobson, 1997).

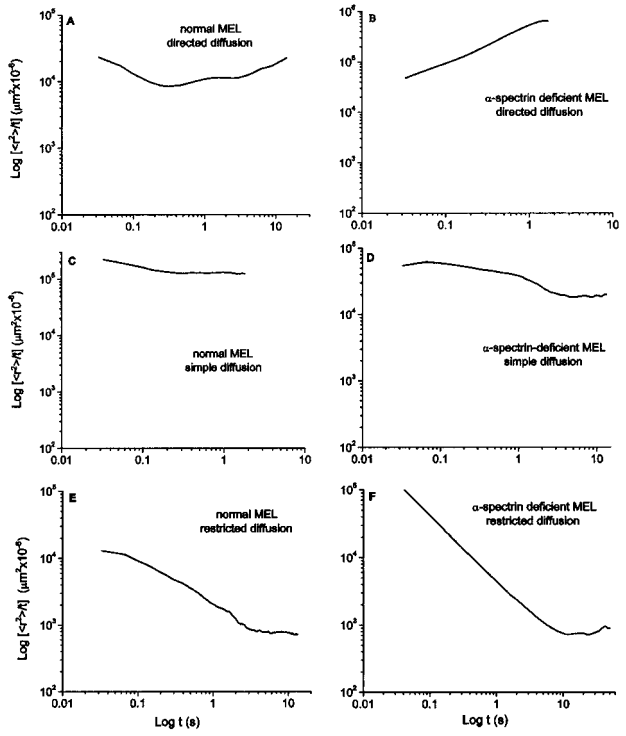

FIGURE 6 Anomalous analysis for particles of different diffusion modes on normal and α-spectrin-deficient MEL cells. *A*, *C*, and *E* are normal MEL cells; *B*, *D*, and *F* are α-spectrin-deficient MEL cells. *A* and *B* are directed diffusion; *C* and *D* are simple diffusion; *E* and *F* are restricted diffusion. *X* axis and *y* axis are logarithmic scale.

DISCUSSION

The diffusion coefficient of class I MHC molecules in α-spectrin-deficient MEL cell surfaces is not significantly different from that in normal MEL cell surfaces, whether measured by FRAP or by SPT (Table 2). Although we did see ~twofold difference in lateral diffusion coefficients by SPT, it is far smaller than the 10- to 50-fold difference, measured in cytoskeleton-defective erythrocytes (Corbett at al., 1994; Golan and Veatch, 1980; Sheetz at al., 1980; Tsuji and Ohnishi, 1986).

In our experiments, we measured the lateral diffusion of class I MHC molecules on three scales: A), large scale: the lateral diffusion of class I MHC molecules (D_{FRAP} from FRAP) as the average diffusion coefficient of many molecules entering and leaving the measured area, typically 0.8 μm radius; the timescale here is tens of seconds; B), medium scale: apparent lateral diffusion of class I MHC molecules over adjacent confinement areas (D_{macro} from SPT); the timescale here is 1–10s; and C), small scale: the lateral diffusion of class I MHC molecules (D_{micro} from SPT) within a confinement area, 330 nm diagonal length on normal MEL cells, or 650 nm diagonal length on α-spectrin-deficient MEL cells. The timescale here is around 100 ms.

On the large scale, the lateral diffusion coefficient was not influenced by the deficiency of α-spectrin. One of the possible reasons is that the defective cytoskeleton still hinders the lateral diffusion of class I MHC molecules, even without α-spectrin. Without α-spectrin, the cytoskeleton is fragile. But the binding sites of actin and ankyrin are on β-spectrin (Bennett and Gilligan, 1993). It is possible that there is still a loose cytoskeleton meshwork beneath the plasma membrane of α-spectrin-deficient MEL cells and that this hinders large-scale lateral diffusion. This would also explain the low mobile fraction measured by FRAP.

There is ~10-fold difference between *D* measured by FRAP (D_{FRAP}) and *D* estimated from SPT (D_{macro}). This divergence of values has also been reported by diffusion of class II MHC molecules (Georgiou at al., 2002). We found that the bead labeling itself only reduced D_{FRAP} ~twofold, compared to labeling with Fab. The other factors that account for the difference have not been resolved.

On the medium scale, the lack of α-spectrin contributed to the larger confinement area and higher D_{macro} on mutant MEL cells than on normal cells. Without the α-spectrin, the meshwork is loose and the mesh size is bigger, so the particles need fewer hops between adjacent confinement areas.

On the small scale, we were measuring the lateral diffusion on timescale of 100 ms. The displacement of class I MHC molecules between two adjacent frames (33 ms) was 15–150 nm. It has been reported that the spectrin mesh of erythrocytes is ~77–110 nm in diagonal length (0.003–0.005 μm^2 area) (Takeuchi et al., 1998) by atomic force microscopy or by high-speed SPT (Tomishige at al., 1998).

At our time and spatial resolution, a molecule that hit the boundary of the confinement area and went back to a point within the area in the interval between two adjacent frames would appear to have a shorter path than its actual path. Therefore a lower diffusion coefficient was determined (Saxton, 1995). The time/spatial resolution here may also contribute to the larger value of the confinement area we measured. In our experiments, one resolvable domain could possibly contain an imperfect spectrin/actin mesh, or a few spectrin/actin meshes. The hops among there are not resolvable with our time/spatial resolution. A higher time resolution, e.g., 0.22 ms/frame in Tomishige's high speed SPT, could alleviate this problem (Saxton and Jacobson, 1997; Tomishige at al., 1998).

The smaller-than-expected difference of lateral diffusion on normal and α-spectrin-deficient MEL cells would also suggest other barrier factors, such as proteins anchored to the cytoskeleton. Even with a sparse cytoskeleton meshwork, the anchored proteins could also inhibit lateral diffusion of unanchored class I MHC molecules (Fujiwara at al., 2002).

The perfect spectrin/actin mesh domain size is 77–110 nm. However, the domain size we measured was 330 nm on normal MEL cells and 650 nm on mutant MEL cells. It seems that our time/spatial resolution could not resolve the perfect spectrin/actin mesh domains. To see if the data fit models other than corral model, we checked for anomalous diffusion in our experiments. According to Saxton, the most important factors for the detection of anomalous diffusion are the timescale of the observations (Saxton, 1994), and the detection of a crossover from anomalous diffusion to normal diffusion (Saxton, 1996). FRAP and video rate SPT experiments with a timescale of seconds will probably only see normal diffusion unless the system is very close to the percolation threshold (Saxton, 1994). But if the D is low enough, and the obstacle concentration is close enough to the percolation threshold, anomalous diffusion and the crossover to normal diffusion can be seen in SPT experiments with the usual sampling time of 33 ms.

In our case, the crossover time is 5 s for normal MEL cells and 8 s for mutant MEL cells. There is anomalous diffusion at short time on small spatial scale. This is similar to the observation by Simson et al. (1998) that normal diffusion of neural cell adhesion molecules on fibroblasts and muscle cells was interspersed with $\sim$8 s short periods of confinement, within which the diffusion was anomalous. Many factors may be involved in this anomalous diffusion on the MEL cells we studied: obstruction, binding, hydrodynamic interactions, interactions of extracellular domains, and interactions of intracellular domains with one another and with the membrane skeleton (Saxton, 2001).

In summary, we used FRAP and SPT methods on three timescales to measure the diffusion of class I MHC molecules on normal MEL and mutant MEL cells. Two models, corral model and anomalous diffusion model, were used to fit the data. We found that the diffusion coefficients of molecules on both cells are not distinguishable by FRAP. However, in SPT experiments, when fitted with normal diffusion with confinement, we see twofold difference on D and twofold difference on confinement area. Interestingly, the anomalous exponent on mutant MEL cells is smaller than that on normal MEL cells (0.28 ± 0.13 vs. 0.50 ± 0.21), suggesting more potential wells and traps in mutant MEL cells than in normal MEL cells. It may be that our failure to see a difference by FRAP is due to the higher anomalous diffusion balanced by fewer barriers in mutant MEL cells than in normal MEL cells.

We thank Dr. Steve Dahl for the help with MEL cell biology and Dr. Gerry Sexton and Andrew Nechkin for help with the imaging equipment.

This work was supported by National Institutes of Health grant GM58554 to M. Edidin.

REFERENCES

Axelrod, D., D. E. Koppel, J. Schlessinger, E. Elson, and W. W. Webb. 1976. Mobility measurement by analysis of fluorescence photobleaching recovery kinetics. *Biophys. J.* 16:1055–1069.

Bennett, V., and D. M. Gilligan. 1993. The spectrin-based membrane skeleton and micron-scale organization of the plasma membrane. *Annu. Rev. Cell Biol.* 9:27–66.

Cherry, R. J. 1979. Rotational and lateral diffusion of membrane proteins. *Biochim. Biophys. Acta.* 559:289–327.

Corbett, J. D., P. Agre, J. Palek, and D. E. Golan. 1994. Differential control of band 3 lateral and rotational mobility in intact red cells. *J. Clin. Invest.* 94:683–688.

Dahl, S. C., R. W. Geib, M. T. Fox, M. Edidin, and D. Branton. 1994. Rapid capping in alpha-spectrin-deficient MEL cells from mice afflicted with hereditary hemolytic anemia. *J. Cell Biol.* 125:1057–1065.

Edidin, M. 2001. Shrinking patches and slippery rafts: scales of domains in the plasma membrane. *Trends Cell Biol.* 11:492–496.

Edidin, M., and I. Stroynowski. 1991. Differences between the lateral organization of conventional and inositol phospholipid-anchored membrane proteins. A further definition of micrometer scale membrane domains. *J. Cell Biol.* 112:1143–1150.

Edidin, M., and T. Wei. 1982. Lateral diffusion of H-2 antigens on mouse fibroblasts. *J. Cell Biol.* 95:458–462.

Edidin, M., Y. Zagyansky, and T. J. Lardner. 1976. Measurement of membrane protein lateral diffusion in single cells. *Science.* 191:466–468.

Edidin, M., M. C. Zuniga, and M. P. Sheetz. 1994. Truncation mutants define and locate cytoplasmic barriers to lateral mobility of membrane glycoproteins. *Proc. Natl. Acad. Sci. USA.* 91:3378–3382.

Fujiwara, T., K. Ritchie, H. Murakoshi, K. Metz-Honda, K. Jacobson, and A. Kusumi. 2002. Phospholipids undergo hop diffusion in compartmentalized cell membrane. *J. Cell Biol.* 157:1071–1081.

Georgiou, G., S. S. Bahra, A. R. Mackie, C. A. Wolfe, P. O'Shea, S. Ladha, N. Fernandez, and R. J. Cherry. 2002. Measurement of the lateral diffusion of human MHC class I molecules on HeLa cells by fluorescence recovery after photobleaching using a phycoerythrin probe. *Biophys. J.* 82:1828–1834.

Golan, D. E., and W. Veatch. 1980. Lateral mobility of band 3 in the human erythrocyte membrane studied by fluorescence photobleaching recovery: evidence for control by cytoskeletal interactions. *Proc. Natl. Acad. Sci. USA.* 77:2537–2541.

Jacobson, K., E. Wu, and G. Poste. 1976. Measurement of the translational mobility of concanavalin A in glycerol-saline solutions and on the cell surface by fluorescence recovery after photobleaching. *Biochim. Biophys. Acta.* 433:215–222.

Koppel, D. E., and M. P. Sheetz. 1981. Fluorescence photobleaching does not alter the lateral mobility of erythrocyte membrane glycoproteins. *Nature*. 293:159–161.

Koppel, D. E., M. P. Sheetz, and M. Schindler. 1981. Matrix control of protein diffusion in biological membranes. *Proc. Natl. Acad. Sci. USA*. 78:3576–3580.

Kusumi, A., Y. Sako, and M. Yamamoto. 1993. Confined lateral diffusion of membrane receptors as studied by single particle tracking (nanovid microscopy). Effects of calcium-induced differentiation in cultured epithelial cells. *Biophys. J*. 65:2021–2040.

Lee, G. M., A. Ishihara, and K. A. Jacobson. 1991. Direct observation of brownian motion of lipids in a membrane. *Proc. Natl. Acad. Sci. USA*. 88:6274–6278.

Ozato, K., T. H. Hansen, and D. H. Sachs. 1980. Monoclonal antibodies to mouse MHC antigens. II. Antibodies to the H-2Ld antigen, the products of a third polymorphic locus of the mouse major histocompatibility complex. *J. Immunol*. 125:2473–2477.

Qian, H., M. P. Sheetz, and E. L. Elson. 1991. Single particle tracking. Analysis of diffusion and flow in two-dimensional systems. *Biophys. J*. 60:910–921.

Saxton, M. J. 1994. Anomalous diffusion due to obstacles: a Monte Carlo study. *Biophys. J*. 66:394–401.

Saxton, M. J. 1995. Single-particle tracking: effects of corrals. *Biophys. J*. 69:389–398.

Saxton, M. J. 1996. Anomalous diffusion due to binding: a Monte Carlo study. *Biophys. J*. 70:1250–1262.

Saxton, M. J. 1997. Single-particle tracking: the distribution of diffusion coefficients. *Biophys. J*. 72:1744–1753.

Saxton, M. J. 2001. Anomalous subdiffusion in fluorescence photobleaching recovery: a Monte Carlo study. *Biophys. J*. 81:2226–2240.

Saxton, M. J., and K. Jacobson. 1997. Single-particle tracking: applications to membrane dynamics. *Annu. Rev. Biophys. Biomol. Struct*. 26:373–399.

Schindler, M., D. E. Koppel, and M. P. Sheetz. 1980. Modulation of membrane protein lateral mobility by polyphosphates and polyamines. *Proc. Natl. Acad. Sci. USA*. 77:1457–1461.

Sheetz, M. P. 1983. Membrane skeletal dynamics: role in modulation of red cell deformability, mobility of transmembrane proteins, and shape. *Semin. Hematol*. 20:175–188.

Sheetz, M. P., M. Schindler, and D. E. Koppel. 1980. Lateral mobility of integral membrane proteins is increased in spherocytic erythrocytes. *Nature*. 285:510–511.

Simson, R., B. Yang, S. E. Moore, P. Doherty, F. S. Walsh, and K. A. Jacobson. 1998. Structural mosaicism on the submicron scale in the plasma membrane. *Biophys. J*. 74:297–308.

Smith, P. R., I. E. Morrison, K. M. Wilson, N. Fernandez, and R. J. Cherry. 1999. Anomalous diffusion of major histocompatibility complex class I molecules on HeLa cells determined by single particle tracking. *Biophys. J*. 76:3331–3344.

Takeuchi, M., H. Miyamoto, Y. Sako, H. Komizu, and A. Kusumi. 1998. Structure of the erythrocyte membrane skeleton as observed by atomic force microscopy. *Biophys. J*. 74:2171–2183.

Tomishige, M., Y. Sako, and A. Kusumi. 1998. Regulation mechanism of the lateral diffusion of band 3 in erythrocyte membranes by the membrane skeleton. *J. Cell Biol*. 142:989–1000.

Tsuji, A., K. Kawasaki, S. Ohnishi, H. Merkle, and A. Kusumi. 1988. Regulation of band 3 mobilities in erythrocyte ghost membranes by protein association and cytoskeletal meshwork. *Biochemistry*. 27:7447–7452.

Tsuji, A., and S. Ohnishi. 1986. Restriction of the lateral motion of band 3 in the erythrocyte membrane by the cytoskeletal network: dependence on spectrin association state. *Biochemistry*. 25:6133–6139.

Wolf, D. E. 1989. Fluorescence microscopy of living cells in culture. *In* Methods in Cell Biology. D. L. Taylor and Y. Wang, editors. Academic Press, San Diego. 271–306.

Wolf, D. E., M. Edidin, and P. R. Dragsten. 1980. Effect of bleaching light on measurements of lateral diffusion in cell membranes by the fluorescence photobleaching recovery method. *Proc. Natl. Acad. Sci. USA*. 77:2043–2045.

Yechiel, E., and M. Edidin. 1987. Micrometer-scale domains in fibroblast plasma membranes. *J. Cell Biol*. 105:755–760.